Multi-Wavelength Visible Light Communication System Design

Pankil M. Butala, Hany Elgala, Thomas D.C. Little
Department of Electrical and Computer Engineering
Boston University, Boston, MA, USA
{pbutala, helgala, tdcl}@bu.edu

Payman Zarkesh-Ha
Department of Electrical and Computer Engineering
University of New Mexico, Albuquerque, NM, USA
payman@ece.unm.edu

Visible light communications (VLC) are achieved by modulation of one or more spectral components in the visible spectrum (≈400-800 nm). The use of this range provides an opportunity to exploit an otherwise untapped medium that is used in human lighting. Most visible light communication systems constructed to date focus on using a broad visible band generated by phosphor-converted blue light emitting diodes, or by filtering to isolate the blue components from these sources. Multi-wavelength systems consider multiple wavelength bands that are combined to produce the desired spectrum realizing a desired color temperature and intensity. The use of multiple bands is also a form of wavelength-division multiplexing. In this paper, we investigate the relationships between the colors comprising the lighting source for a range of lighting states, the spectral separation of communication channels, the relative intensities required to realize lighting states, how modulation can be most effectively mapped to the available color channels, and the design of an optical filtering approach to maximize SNR while minimizing crosstalk at the receiver. Simulation results based on a three colored VLC system are discussed using orthogonal frequency division multiplexing for each color. We show that the system is the most power efficient at 6250 K correlated color temperature, with transmitter spectral spread of 5 nm and filter transmittance width of 40 nm.

Keywords—Visible Light Communications (VLC), Optical Wireless Communications (OWC), Multiple Input Multiple Output (MIMO), Wavelength Division Multiplexing (WDM), Orthogonal Frequency Division Multiplexing (OFDM).

I. Introduction

There has been a rapid increase in use of networked portable computing devices in recent years. These devices are consuming increasingly more information in the form of multimedia streaming [1]. Trying to keep up with this increasing demand for wireless data has strained the network infrastructure thus creating the phenomenon of 'spectrum crunch'. Its effect can be seen in reduced quality of service and lower download speeds.

On the other hand, advances made by the solid state industry has created energy efficient illumination devices called light emitting diodes (LED). The intensity of radiant flux emitted by LEDs can be modulated at a high enough rate such that information transfer can be achieved at relatively high speeds while the intensity variations are invisible to human eye. One or more LEDs can be packaged together to form a 'luminaire' which under the above model services the dual functionality of providing wireless network access and maintaining illumination [2]. The additional downlink capacity provided by such "smart" luminaires can help mitigate some of the aforementioned spectrum crunch.

A simple single input single output visible light communications (VLC) channel can be created by using an LED as a transmitter and a photodiode as a receiver. Channel characteristics for an optical channel are described in reference [3]. Another way of improving the capacity of a wireless channel is by using multiple transmitting and receiving elements in a multiple input multiple output (MIMO) configuration. Different types of MIMO systems [4–8] have been reported in literature.

One type of an optical MIMO system is wavelength division multiplexed (WDM) VLC system. Different WDM system prototypes have been reported in literature [9–11]. These describe an instance of a WDM system without analysis of the optimal operating point. In this work, design of multi-wavelength VLC systems under lighting constraints when correlated color temperature (CCT) of illumination, transmitter spectral power distribution (SPD) and receivers' filter spectral transmittance full width at half maximum (FWHM) are varied, is studied for the first time. Simulations for a three colored WDM VLC system then provide numerical analysis of the system performance giving an insight into optimal design criteria. For the system considered, we find that its most power efficient operation occurs at CCT of 6250 K, narrow transmitting elements' SPD (5 nm), and receiver filter FWHM of 40 nm.

The following notations are used in this paper. Scalar values are represented in regular font. Vectors and matrices are represented in bold font. Conjugate transpose of $\mathbf{A}$ is represented by $\mathbf{A}^*$. Operators $:=$ and $||.||$ represent definition and euclidean norm respectively.

An introduction to optical MIMO systems is provided in Section II. WDM, a subset of optical MIMO systems, is introduced in Section III. Section IV describes the simulation setup. Results and discussion is provided in Section V. Conclusions are then drawn in Section VI.

II. Optical MIMO Channel

This section provides an introduction to an optical MIMO channel that can be established between multiple optical transmitting and receiving elements. Multiple transmitting elements can be established over dimensions such as space,

time, frequency, wavelength, polarization, and others. Each receiving element must produce an output electrical signal that is proportional to the radiant flux incident on it from the dimension of interest. A typical optical MIMO channel can be modeled as a linear time invariant system and represented as

$$\mathbf{Y} = \mathbf{HX} + \mathbf{W} \tag{1}$$

$\mathbf{X}$ is an N_{tx} dimensional vector. Each element of $\mathbf{X}$ represents the radiant flux emitted by each transmitting element. $\mathbf{Y}$ is an N_{rx} dimensional vector. Each element of $\mathbf{Y}$ represents the signal output from each receiving element. $\mathbf{H}$ is an $N_{rx} \times N_{tx}$ dimensional channel matrix. Each element $h_{ij} \in \mathbf{H}$; $i \in \{1, 2, \ldots, N_{rx}\}$, $j \in \{1, 2, \ldots, N_{tx}\}$ represents the conversion factor for signal output from the i^{th} receiving element when radiant flux from j^{th} transmitting element is incident on it after including the path losses. $\mathbf{W}$ is an N_{rx} dimensional noise vector. It is typically modeled as additive white Gaussian noise independent of transmitted vector $\mathbf{X}$ i.e. $\mathbf{W} \sim \mathcal{N}(\mathbf{0}, \sigma_n^2 \mathbf{I}_{N_{rx}})$.

The amount of radiant flux per solid angle emitted by a transmitting element in a certain angular direction ϕ is given by the angular radiant intensity distribution. An LED's radiant intensity distribution is usually characterized by a Lambertian distribution and is given by

$$L_m(\phi) = \begin{cases} \frac{(m+1)}{2\pi} cos^m(\phi) & ; -\pi/2 \leq \phi \leq \pi/2 \\ 0 & ; \text{ else} \end{cases} \tag{2}$$

If $\Phi_{\frac{1}{2}}$ is the emission angle at which radiant intensity of a transmitting element is half its peak value (at $\phi = 0^\circ$), the Lambertian order of that emission is $m = -ln(2)/ln(cos(\Phi_{\frac{1}{2}}))$.

A photodiode is a device that produces an electrical signal output that is proportional to the radiant flux incident on it. The photodiode effective area can be increased by using concentrator optics and this gain is given by

$$G_\eta(\psi) = \begin{cases} \frac{\eta^2}{sin^2(\Psi_{\frac{1}{2}})} & ; 0 \leq \psi \leq \Psi_{\frac{1}{2}} \leq \frac{\pi}{2} \\ 0 & ; \psi > \Psi_{\frac{1}{2}} \end{cases} \tag{3}$$

where ψ is the angle of incidence of the flux, η is the refractive index of the material that the optics are made of, and $\Psi_{\frac{1}{2}}$ is the half angle of the field of view of the concentrator.

Optical filters may be used at the receiver to acquire the wavelengths of interest while rejecting the ambient radiation. Depending on the type of filter used, its transmittance may be a function of the angle of incidence ψ. Let $T(\psi, \lambda)$ be the transmittance of an optical filter. If $S(\lambda)$ is the normalized SPD of incident radiation and $R(\lambda)$ is the responsivity of the receiving photodiode, the effective responsivity of the receiving element is given by

$$R_e(\psi) = G_\eta(\psi) \int_{\lambda_{min}}^{\lambda_{max}} S(\lambda) T(\psi, \lambda) R(\lambda) d\lambda \tag{4}$$

Let $\mathbf{d}_{ij}$ be the vector from i^{th} receiving element to j^{th} transmitting element. The distance between the two is then given by $||\mathbf{d}_{ij}||$. The channel gain from the i^{th} receiving element to the j^{th} transmitting element is given by

$$h_{ij} = L_{m_j}(\phi_{ij}) \frac{A_i}{||\mathbf{d}_{ij}||^2} cos(\psi_{ij}) R_{e_i}(\psi_{ij}) \tag{5}$$

where m_j is the Lambertian order of the j^{th} transmitting element, ϕ_{ij} and ψ_{ij} are the angles subtended between vector $\mathbf{d}_{ij}$ and surface normals respectively of the j^{th} transmitting and i^{th} receiving elements, and A_i is the active area of the photodiode on the i^{th} receiving element. The h_{ij} thus computed are the elements of the channel matrix $\mathbf{H}$.

Ambient light incident on a photodiode generates shot noise. Let $P_a(\lambda)$ be SPD of isotropic ambient light. This would generate shot noise in a receiving element with variance

$$\sigma_{sh}^2 = \frac{2qAG_\eta(\psi)}{\Psi_{\frac{1}{2}}} \int_{\lambda_{min}}^{\lambda_{max}} \int_0^{\Psi_{\frac{1}{2}}} P_a(\lambda) T(\psi, \lambda) R(\lambda) d\psi d\lambda \tag{6}$$

where q is the charge of an electron. Shot noise statistics are typically modeled as a Poisson distribution.

A trans-impedance amplifier (TIA) is most often used as the first stage amplifier. Thermal noise is the most dominant component of TIA electrical noise. The thermal noise variance as described in reference [3] is given by

$$\sigma_{th}^2 = \frac{4kT}{R_f} \tag{7}$$

where constant k is Boltzmann constant, T is the absolute temperature, and R_f is the TIA feedback resistance. Thermal noise statistics are typically modeled as a Gaussian distribution.

Total input referred noise variance is usually approximated as the sum of shot noise variance and thermal noise variance. For sake of mathematical simplicity, total noise is assumed to have Gaussian statistics with mean 0 and variance $\sigma_n^2 = \sigma_{sh}^2 + \sigma_{th}^2$.

In VLC, transmitting elements perform dual function of providing wireless data transmission while maintaining illumination levels. To perform a fair comparison between different modulation systems operating at same illumination levels needs a different definition of signal to noise ratio (SNR). In this work, SNR is defined as the ratio of the average transmitted electrical power to noise power and is similar as in reference [12].

$$SNR_{avg}^{tx} := \frac{(eP_{avg}^{tx})^2}{\sigma_n^2} \tag{8}$$

where P_{avg}^{tx} is the average radiant flux emitted by a transmitter, e is the optical to electrical conversion factor $(AW^{-1}\Omega^{-2})$ and σ_n^2 is the noise power. Parameter e is assumed to be 1 without loss of generality.

III. Wavelength Division Multiplexing

With recent advances in solid state technology, LEDs have emerged as the most energy efficient sources for illumination. SPD of different colored LEDs that emit different narrow-band spectrum can be combined in different ratios to produce different colors for illumination including the shades of white on the black body radiation curve. The ability to combine multiple narrow band sources to generate white light also provides the benefit of being able to transmit concurrent information streams over different color groups; thus enabling WDM. The performance of a multi-colored VLC system depends on a number of parameters including SPD of the transmitting

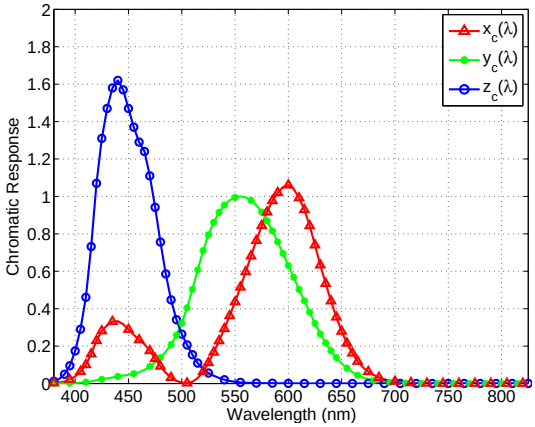

Fig. 1. CIE XYZ 1931 model color matching functions

elements, illumination color, filter transmission function, and receiver responsivity.

Lasers and LEDs produce a much smaller SPD width as compared to incandescent and fluorescent sources and are thus preferable for WDM. LED emission can be modeled with a Gaussian distribution as in Eq. (9a) while laser emission can be modeled with a Lorentzian distribution as in Eq. (9b). Equations in (9) model emission spectra for the j^{th} transmitting element.

$$S_j(\lambda) = \frac{1}{\sqrt{2\pi\sigma_j^2}} exp\left[-\frac{(\lambda-\lambda_j)^2}{2\sigma_j^2}\right] \tag{9a}$$

$$S_j(\lambda) = \frac{1}{\pi}\frac{0.5\Gamma_j}{(\lambda-\lambda_j)^2+(0.5\Gamma_j)^2} \tag{9b}$$

where λ_j is the dominant wavelength of emission, σ_j is the measure of spread (deviation) from the dominant wavelength for the Gaussian model, and Γ_j is the FWHM from the dominant wavelength for the Lorentzian model. At small SPD width, most of the optical power is emitted at the dominant wavelength. At larger SPD widths the optical power is spread across a larger wavelength range and starts overlapping across different transmitting elements, thus causing interference.

To generate white light $W(\lambda)$, emissions from different transmitting elements are weighted by factor t_j before being mixed together. The resulting spectrum is given by

$$W(\lambda) = \sum_{j=1}^{N_{tx}} t_j S_j(\lambda) \tag{10}$$

The *commission internationale de l'éclairage* (CIE) specified the CIE 1931 XYZ color space. It maps an SPD to a color representation as sensed by the human eye. The standard defines three color matching functions $x_c(\lambda)$, $y_c(\lambda)$, and $z_c(\lambda)$ as shown in Fig. 1. The tristimulus values for the XYZ primaries are given by

$$X_W = \int_{\lambda_{min}}^{\lambda_{max}} W(\lambda)x_c(\lambda)d\lambda \tag{11a}$$

$$Y_W = \int_{\lambda_{min}}^{\lambda_{max}} W(\lambda)y_c(\lambda)d\lambda \tag{11b}$$

$$Z_W = \int_{\lambda_{min}}^{\lambda_{max}} W(\lambda)z_c(\lambda)d\lambda \tag{11c}$$

A color can be expressed in terms of its chromaticity and luminance. Chromaticity coordinates capture the hue and saturation of the color while luminance captures the amount of light in the color. The chromaticity coordinates for the SPD can be then be computed from the tristimulus values as

$$\begin{bmatrix} x \\ y \end{bmatrix} = \frac{1}{X_W + Y_W + Z_W}\begin{bmatrix} X_W \\ Y_W \end{bmatrix} \tag{12}$$

The spectral radiance of a black body heated to temperature T as stated by Planck's law is given by

$$S(\lambda) = \frac{2hc^2}{\lambda^5\left[exp\left(\frac{hc}{\lambda kT}\right)-1\right]} \tag{13}$$

where h is the Planck's constant, c is speed of light, and k is Boltzmann's constant. Replacing $W(\lambda) = S(\lambda)$ in Eq.(11) and then from Eq.(12) we obtain the CIE 1931 XYZ chromaticity values $[x, y]$ associated with a black body heated to temperature T. In this context T is also known as the CCT for color represented by $[x, y]$. Note that two different SPDs can generate the same chromaticity coordinates. This is due to the principle of metamerism.

Traditionally luminaires have been specified to generate a certain CCT with colors at lower temperature appearing (ironically) warm than those at higher temperatures. It is practical to generate colors off the black body radiation curve using different colored lasers and LEDs. However for this analysis, we shall stick to colors generated on the black body radiation curve. As the CCT changes from a lower value to a higher value, the optical power available to transmit information on any color channel varies thus affecting the overall communication performance.

Optical filters can be manufactured to permit narrow bandpass filtering with nanometer precision using plasmonics [13–15]. Broad bandpass optical filters that make use of interference are widely available. The transmittance of these filters can be modeled as Lorentzian functions of wavelength. The choice of the filter FWHM is a tradeoff to collect the maximum signal while rejecting interference and background illumination.

Responsivity of the receiving elements also affects the aggregate system performance. It depends on the quantum efficiency of the material of sensor. Reference [16] computes responsivity as

$$R(\lambda) = \frac{\xi\lambda}{1240} \tag{14}$$

where ξ is the quantum efficiency of the material, and λ is wavelength of interest. For equal signal radiant flux, signals that span wavelength ranges with lower responsivity will perform poorly as compared to the rest.

IV. Simulation

Simulations are performed to study how the choice of design parameters like illumination CCT, transmitter SPD, and filter FWHM affect the performance of a multi-colored VLC system. Three transmitting elements with Gaussian emission spectrum at dominant wavelengths of red (627 nm), green (530 nm) and blue (470 nm) are selected. Using these transmitting elements, CCT range of [2500 7000] K is sought. SPD spread within [5 50] nm is considered. Fig.2 illustrates normalized SPDs needed to achieve the range of CCTs for transmitting elements with 5 nm spread. Note that for all CCTs, the transmitted radiant flux may vary to achieve a constant target illumination at receiver.

Unique $t_R : t_G : t_B$ ratios are generated after varying the tristimulus values in the range [0 1] in 0.1 unit steps. By substituting these values in Eq.(10)-Eq.(12), chromaticity coordinates for resulting SPDs are calculated. An initial characterization step generates a pre-populated table consisting of the tristimulus values and corresponding chromaticity coordinates. As the CCT is varied, the chromaticity coordinates are computed as shown in Section III. From the pre-computed table, the tristimulus values that achieve the closest chromaticity are selected. The SPD is then scaled to achieve target illumination (400 lx) at the receiver that is located at a distance of 2 m from the transmitter. The surface normals of the transmitter and receiver are assumed to be parallel.

Optical filter's passband can be designed to center on the transmitting elements' dominant wavelengths. Optical filters for the simulation are modeled to have Lorentzian transmittance with ideal value 1 at the dominant red, green and blue wavelengths mentioned above. Filter transmittance as a function of wavelength is illustrated in Fig.3. Filter FWHM considered for the analysis lie in [1 250] nm range.

The receiver sensor is assumed to be made of silicon. The assumed quantum efficiencies and responsivity of the sensor taken from source [17] is illustrated in Fig.4. The responsivity near the blue wavelength is about 0.29 A.W^{-1} and increases steadily to about 0.46 A.W^{-1} near the red before rapidly reducing as the energy of the incident photon approaches the bandgap energy of silicon.

To analyze the system performance, one can start with

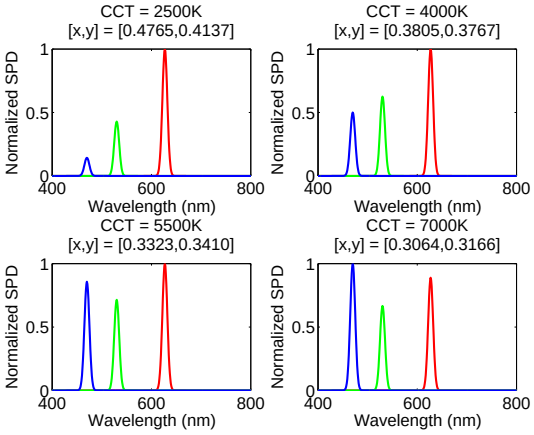

Fig. 2. Transmitting element normalized spectral power distribution

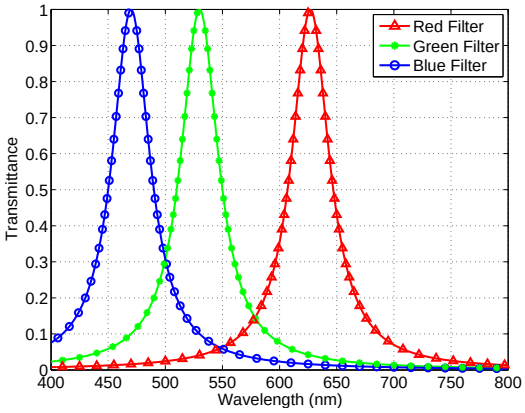

Fig. 3. Filter transmittance for full width at half maximum = 40nm

the system model as described in Eq. (1). A random bit stream is then generated. Bits for each link are then using asymmetrically clipped offset and DC-biased optical orthogonal frequency division multiplexing (ACO-OFDM and DCO-OFDM). Details on these optical OFDM techniques can be found in references [18], [19]. For this simulation, ACO-OFDM and DCO-OFDM are implemented with 64 sub-carriers and 64-QAM and 8-QAM modulation respectively. This ensures that both schemes achieve similar bits/symbol with ACO-OFDM achieving 96 bits/symbol and DCO-OFDM achieving 93 bits/symbol. The DC level on each link is set to ensure the desired CCT is achieved at the 400 lx illumination level. This generates the transmit vector $\mathbf{X}$.

Having established $N_{tx} = 3$ transmitting and $N_{rx} = 3$ receiving elements, the 3×3 channel matrix $\mathbf{H}$ can be computed as in Section II. Additive white Gaussian noise vector $\mathbf{W}$ is generated and is then added to the transmitted vector. With the knowledge of the transmitted signal power and by varying the receiver noise, simulations over a range of SNR_{avg}^{tx} are carried out. Vector $\mathbf{Y}$ then collects the received signal and the added noise and interference. The least squares estimate of the transmitted signal vector is computed as

$$\hat{\mathbf{X}} = (\mathbf{H}^*\mathbf{H})^{-1}\mathbf{H}^*\mathbf{Y} \tag{15}$$

An estimate of the transmitted optical OFDM frame for each color is obtained by aggregating least squares estimates of

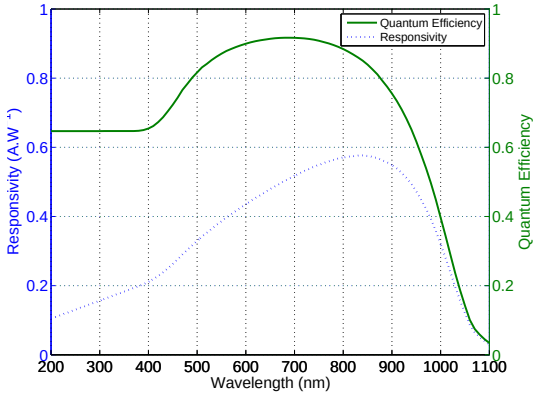

Fig. 4. Receiver quantum efficiency and responsivity [17]

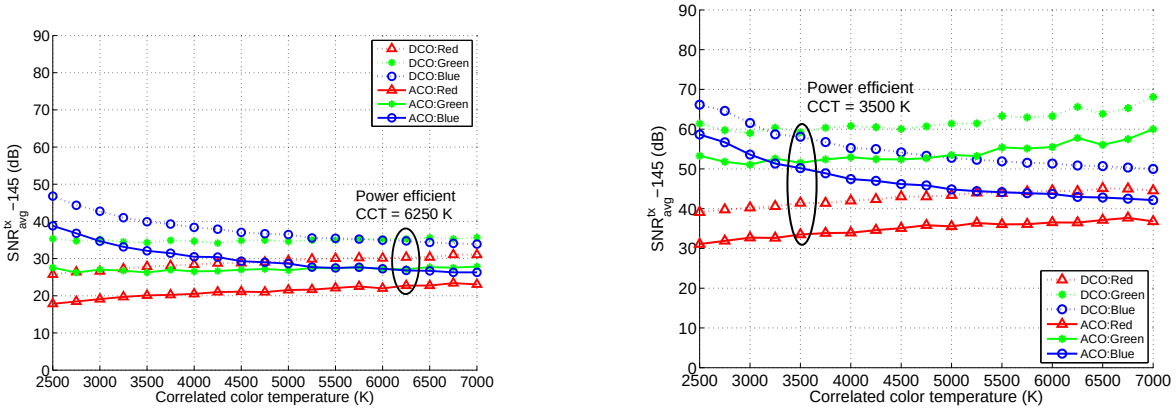

(a) Most power efficient operation point

(b) High inter-channel interference

Fig. 5. SNR^{tx}_{avg} vs correlated color temperature to achieve BER $\leq 10^{-3}$
(a) Transmitter: $\sigma_r = \sigma_g = \sigma_b = 5$ nm; Filter: $\Gamma_r = \Gamma_g = \Gamma_b = 40$ nm (b) Transmitter: $\sigma_r = \sigma_g = \sigma_b = 50$ nm; Filter: $\Gamma_r = \Gamma_g = \Gamma_b = 250$ nm

the received signal vectors. Further signal processing on each optical OFDM frame gets an estimate of the transmitted QAM symbol. Decoding the QAM symbols provides an estimate of the transmitted bits. BER is then calculated by comparing the transmit and estimated bit streams.

V. Results and Discussion

As mentioned before, system performance versus the choice of illumination SPD, transmitter SPD spread, and filter transmittance FWHM as described in Section IV are studied. For each unique configuration yielded by varying the parameters, BER versus SNR^{tx}_{avg} is empirically determined using monte-carlo simulations. Based on the simulation setup, the path loss from the transmitting elements to the receiving elements is about 145 dB. To plot the change in system performance when each parameter is varied, the minimum SNR^{tx}_{avg} needed to achieve target BER $\leq 10^{-3}$ is selected. Since ACO-OFDM is more power efficient compared to DCO-OFDM, for all the cases discussed below, ACO-OFDM needs lower transmit signal power to achieve the target BER as compared to DCO-OFDM.

The change in performance of the red, green and blue links as the CCT is varied from 2500 K to 7000 K is shown in Fig.5. At 2500K, the SPD has a greater contribution from red, then green and then blue. Thus the red link achieves target BER at lower transmitted signal power. As the CCT increases, relative signal power from the red link decreases, that of the green remains similar, and that of the blue increases. Thus the amount of aggregate transmit flux needed to achieve target BER from the red link starts increasing, that of the green remains relatively unchanged, while that of the blue decreases with increase in CCT. For the specified multi-colored system, CCT = 6250 K provides the most power efficient operating point as illustrated in Fig.5a. Increasing the transmitting elements' SPD or the filter FWHM introduces increasingly more inter-channel interference (ICI). This causes the most power efficient operating point to shift towards CCT = 3500 K but with greater power requirements as seen in Fig.5b.

The change in performance of the red, green and blue links as the transmitting element SPD spread is varied from 5 nm to 50 nm is shown in Fig.6. As the SPD spread is increased, the performance of all three links degrade. This can be attributed to two factors. Initially, as the signal power is distributed across a larger wavelength range, with the filter transmittance function remaining the same, increasingly more signal gets rejected by the filter. Thus the receiver collects a smaller fraction of the signal power, degrading the performance. Secondly, as the individual SPDs spread enough, they start overlapping and causing ICI. The effect of ICI is more pronounced on the green link because it gets interference from both, red and blue. Thus transmitter consisting of transmitting elements with narrower emission spectra are more power efficient efficient than those with wider emission spectra. However, it is commonly believed that sources with spiky emission spectra do not produce good quality of illumination because objects with reflectance spectra lying outside the spikes in the illumination spectra will be perceived to be poorly lit. If this is the case, the choice of the transmitting elements' SPD spread would be a tradeoff between the communication and illumination performance. For the specified multi-colored system, SPD spread = 5 nm provides the most power efficient operating point.

The change in performance of the red, green and blue links

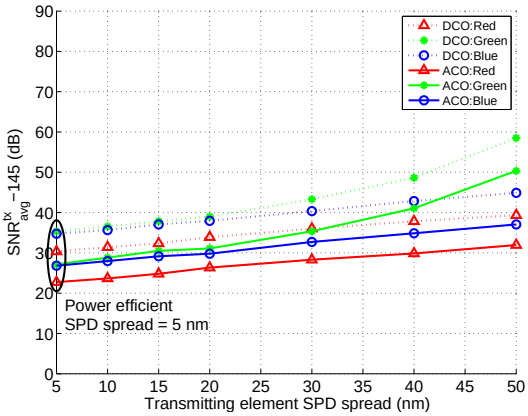

Fig. 6. SNR^{tx}_{avg} vs transmitting element spectral power distribution spread to achieve BER $\leq 10^{-3}$
Filter: $\Gamma_r = \Gamma_g = \Gamma_b = 40$ nm; CCT = 6250 K

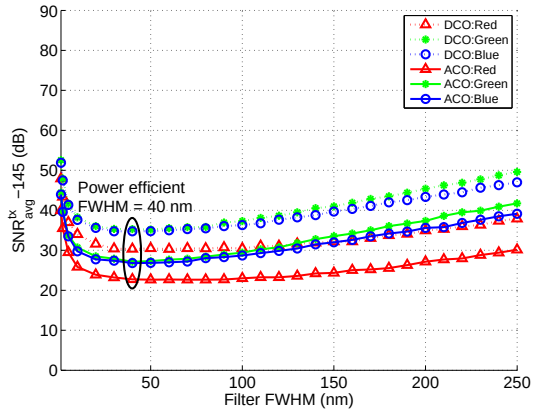

Fig. 7. SNR^{tx}_{avg} vs filter full width at half maximum to achieve BER $\leq 10^{-3}$
Transmitter: $\sigma_r = \sigma_g = \sigma_b = 5$ nm; CCT = 6250 K

as the receiving element filter FWHM is varied from 1 nm to 250 nm is shown in Fig.7. As the filter FWHM increases, initially the system performance improves significantly. At these lower FWHM ranges, the filters transmit a smaller fraction of the signal to the sensors and thus performance is limited by the amount of signal power collected for each link. At higher FWHM ranges, along with additional signal, the filters permit increasingly more ambient light and interference from neighboring links, thus degrading the performance. For the specified multi-colored system, filter FWHM = 40 nm provides the most power efficient operating point.

VI. Conclusion

In this work, we introduced wavelength division multiplexing visible light communication system in the context of variable illumination constraints. We then analyzed how variations in correlated color temperature, transmitter spectral power distribution, and the receiver filter transmittance affect the communication performance of such a system. For the three colored system considered, the blue and the green links pose the performance bottlenecks because of the relatively lower contribution to the SPD and lower photodiode responsivity as compared to the red. As the ICI increases, the most power efficient CCT shifts towards lower temperatures. Transmitting elements with the smallest spectral spread provide the most power efficient operating point. The effect of increase in spectral spread is most pronounced in the green link because it suffers the most from interference from the blue and red links. Filters with narrow transmittance reject a lot of the signal power while filters with a broad transmittance accept a lot of interference. Both of these affect the power efficiency of the system. For the setup considered, least power efficient operating point is for DCO-OFDM at CCT = 2500 K, transmitting element SPD spread = 50 nm, and filter FWHM = 1 nm. The most power efficient operating point is for ACO-OFDM at CCT = 6250 K, transmitting element SPD spread = 5 nm, and filter FWHM = 40 nm.

VII. Acknowledgement

This work was supported by the Engineering Research Centers Program of the National Science Foundation under NSF Cooperative Agreement No. EEC-0812056.

References

[1] (2014, June) Cisco visual networking index: Forecast and methodology, 2013-2018. White Paper. Cisco.

[2] T. Komine and M. Nakagawa, "Fundamental analysis for visible-light communication system using led lights," *Consumer Electronics, IEEE Transactions on*, vol. 50, no. 1, pp. 100 – 107, feb 2004.

[3] J. Kahn and J. Barry, "Wireless infrared communications," *Proceedings of the IEEE*, vol. 85, no. 2, pp. 265 –298, feb 1997.

[4] S. Hranilovic and F. Kschischang, "A pixelated mimo wireless optical communication system," *Selected Topics in Quantum Electronics, IEEE Journal of*, vol. 12, no. 4, pp. 859 –874, july-aug. 2006.

[5] L. Zeng, D. O'Brien, H. Minh, G. Faulkner, K. Lee, D. Jung, Y. Oh, and E. T. Won, "High data rate multiple input multiple output (mimo) optical wireless communications using white led lighting," *Selected Areas in Communications, IEEE Journal on*, vol. 27, no. 9, pp. 1654 –1662, december 2009.

[6] A. Ashok, M. Gruteser, N. Mandayam, J. Silva, M. Varga, and K. Dana, "Challenge: mobile optical networks through visual mimo," in *Proceedings of the sixteenth annual international conference on Mobile computing and networking*, ser. MobiCom '10. New York, NY, USA: ACM, 2010, pp. 105–112.

[7] P. M. Butala, H. Elgala, and T. D. Little, "Svd-vlc: A novel capacity maximizing vlc mimo system architecture under illumination constraints," in *Globecom Workshops (GC Wkshps), 2013 IEEE*, Dec 2013, pp. 1087–1092.

[8] P. M. Butala, H. Elgala, and T. D. Little, "Sample indexed spatial orthogonal frequency division multiplexing," *Chinese Chemical Letters*, vol. 12, no. 9, 2014.

[9] K. Wang, A. Nirmalathas, C. Lim, and E. Skafidas, "4 12.5 gb/s wdm optical wireless communication system for indoor applications," *Lightwave Technology, Journal of*, vol. 29, no. 13, pp. 1988 –1996, july1, 2011.

[10] C. Kottke, J. Hilt, K. Habel, J. Vučić, and K.-D. Langer, "1.25 gbit/s visible light wdm link based on dmt modulation of a single rgb led luminary," in *European Conference and Exhibition on Optical Communication*. Optical Society of America, 2012, p. We.3.B.4.

[11] G. Cossu, A. M. Khalid, P. Choudhury, R. Corsini, and E. Ciaramella, "3.4 gbit/s visible optical wireless transmission based on rgb led," *Opt. Express*, vol. 20, no. 26, pp. B501–B506, Dec 2012.

[12] T. Fath and H. Haas, "Performance comparison of mimo techniques for optical wireless communications in indoor environments," *Communications, IEEE Transactions on*, vol. 61, no. 2, pp. 733–742, 2013.

[13] T. Xu, Y.-K. Wu, X. Luo, and L. J. Guo, "Plasmonic nanoresonators for high-resolution colour filtering and spectral imaging," *Nature Communications*, vol. 1, no. 59, August 2010.

[14] Q. Chen, D. Das, D. Chitnis, K. Walls, T. Drysdale, S. Collins, and D. Cumming, "A cmos image sensor integrated with plasmonic colour filters," *Plasmonics*, vol. 7, no. 4, pp. 695–699, 2012.

[15] S. Yokogawa, S. P. Burgos, and H. A. Atwater, "Plasmonic color filters for cmos image sensor applications," *Nano Letters*, vol. 12, no. 8, pp. 4349–4354, 2012.

[16] S. R. Z. Ghassemlooy, W. Popoola, *Optical Wireless Communications: System and Channel Modelling with MATLAB*, T. . F. Group, Ed. CRC Press, August 2012.

[17] C. Honsberg and S. Bowden. Quantum efficiency. PVEducation.org. [Online]. Available: http://www.pveducation.org/pvcdrom/solar-cell-operation/quantum-efficiency

[18] J. Carruthers and J. Kahn, "Multiple-subcarrier modulation for nondirected wireless infrared communication," *Selected Areas in Communications, IEEE Journal on*, vol. 14, no. 3, pp. 538–546, 1996.

[19] J. Armstrong and A. Lowery, "Power efficient optical ofdm," *Electronics Letters*, vol. 42, no. 6, pp. 370 – 372, march 2006.